Journal of Water Process Engineering 80 (2025) 109152

Contents lists available at ScienceDirect

Journal of Water Process Engineering

journal homepage: www.elsevier.com/locate/jwpe

Sustainable sodium alginate-La-Al-MOFs composite beads with enhanced mechanical strength for fluoride removal

Zi Song [a,b], Ze Wang [c,a], Fei Yang [a,b], Huu Hao Ngo [a,d], Wenshan Guo [a,d,*], Xinbo Zhang [a,b,*]

[a] Joint Research Centre for Protective Infrastructure Technology and Environmental Green Bioprocess, School of Environmental and Municipal Engineering, Tianjin Chengjian University, Tianjin, 300384, China
[b] Tianjin Key Laboratory of Aquatic Science and Technology, Tianjin Chengjian University, Jinjing Road 26, Tianjin, 300384, China
[c] Long Jiang Environmental Protection Group Co., Ltd, Harbin, 150090, China
[d] Centre for Technology in Water and Wastewater, School of Civil and Environmental Engineering, University of Technology Sydney, Sydney, NSW, 2007, Australia

ARTICLE INFO

Editor: Luca Fortunato

Keywords:
Adsorption
Fluoride removal
Sodium alginate
La-Al-MOFs

ABSTRACT

Excessive fluoride has detrimental effects on human health and contributes to the contamination of aquatic and terrestrial environments. However, conventional powdered fluoride adsorbents often suffer from challenges such as poor recyclability and secondary pollution. Herein, a bimetallic Metal-organic frameworks (MOF) composite was synthesized employing a hydrothermal method and then embedded in sodium alginate to form sodium alginate-La-Al-MOFs composite beads (SAMB) gel spherical material. The fluoride adsorption performance of SAMB was systematically evaluated under varying conditions. SAMB demonstrated strong removal performance over an extensive pH spectrum, ranging from 3 to 9, with optimal performance observed at pH 3. At an initial fluoride concentration of 20 mg/L and an adsorbent dosage of 1 g/L, SAMB achieved a maximum fluorine removal efficiency of 87.6 %. Fluoride adsorption followed monomolecular layer chemisorption as confirmed by Langmuir and pseudo-secondary kinetics. The large surface pores of SAMB enabled rapid removal of fluoride within 15 min with a maximum adsorption capacity of 46.67 mg/g at 298.15 K. Regeneration experiments displayed the adsorption efficiency of the gel spheres adsorbent only decreased by 29 % after four times of reuse. The adsorption mechanism revealed that SAMB fluorine adsorption was dominated by ion exchange and electrostatic attraction. These findings demonstrate that SAMB serves as an effective and environmentally benign adsorbent for aqueous fluoride removal, offering a sustainable alternative to conventional treatment methods.

1. Introduction

Fluorine is a chemically active halogen, often stored in rock-containing, fluorine ores (e.g. fluorite CaF_2, cryolite Na_3AlF_6), with the weathering of fluorine-containing minerals, fluorine is released into the groundwater, which is the main source of fluorine pollution [1]. Industrial production processes such as steelmaking, ceramics, glass and semiconductors also produce large amounts of fluoride waste liquid. While the World Health Organization (WHO) recommends a maximum fluoride level of 1.5 mg/L for drinking water, the Chinese national standard (GB5749–2006) mandates a more stringent standard of 1 mg/L [2]. Excessive fluoride intake can seriously affect human health, inducing dental fluorosis, osteoporosis, growth retardation and other diseases [3]. Therefore, in the context of rapid industrial and agricultural development, the elimination of fluoride from water represents a significant contemporary challenge [4]. To mitigate fluorine contamination, several feasible methods have been developed, including electrodialysis, membrane technology, adsorption, ion exchange technology, etc. [5,6]. Of the available options, adsorption is extensively employed due to its operational simplicity, economic advantages, and considerable removal effect [7,8].

Common adsorbents for fluoride removal include carbon materials, mineral-based substances, ion-exchange resins, and metal oxides [9]. Carbon materials generally feature high specific surface area and tunable porosity, while conventional activated carbons suffer from limited capacity and selectivity toward fluoride. Novel carbons like

* Corresponding authors at: Joint Research Centre for Protective Infrastructure Technology and Environmental Green Bioprocess, School of Environmental and Municipal Engineering, Tianjin Chengjian University, Tianjin, 300384, China.
E-mail addresses: wguo@uts.edu.au (W. Guo), xinbozhang@tcu.edu.cn (X. Zhang).

https://doi.org/10.1016/j.jwpe.2025.109152
Received 22 September 2025; Received in revised form 6 November 2025; Accepted 16 November 2025
Available online 20 November 2025

graphene show high uptake efficiency, but the practical use is constrained by complex synthesis [10]. Natural minerals (e.g., hydroxyapatite and zeolite) are widely available and cost-effective, yet their inherent adsorption is low. Though modifications such as metal doping or hydrothermal treatment can enhance performance, stability remains unsatisfactory [11]. Ion-exchange resins, with their 3D network and functional groups, allow rapid uptake and easy regeneration, but they exhibit poor fluoride selectivity and are vulnerable to competing anions (e.g., sulfate and chloride), leading to reduced efficacy in real waters [12]. In contrast, metal oxides demonstrate superior selectivity, chemical stability, and affinity for fluoride, enabling efficient and durable defluoridation without introducing secondary contaminants [13].

Metal-organic frameworks (MOFs), a class of nanoporous materials composed of multinuclear metal clusters, have attracted significant research interest in recent years due to their exceptional properties, including high surface area, extensive porosity, high crystallinity, and structurally tunable features [14]. MOFs exhibit extensive potential for application in gas separation processes, air filtration, wastewater treatment, sensing, etc. [15,16]. Particularly, MOFs exhibit highly tunable pore structures and large surface areas, rendering them effective adsorbents for aqueous pollutant removal [17]. However, conventional MOFs often exhibit limited fluoride adsorption capacity due to weak ion affinity and interference from complex water matrices [18]. This performance limitation highlights the need for developing enhanced MOF materials specifically for fluoride removal. In the previous research, Alhassan et al. [19] successfully prepared a composite Bx-Ce-La@ 500 through the incorporation of lanthanum and cerium into bauxite. Their findings demonstrated that the fluorine adsorption of composites was about six times higher than that of the ordinary bauxite. A camellia-like bimetallic MOFs was prepared by Ke et al. [20] for the removal of fluorine from tea bricks by soluble bimetallic competitive coordination combined with alkali-assisted solvothermal method, which presented a fluorine removal efficiency of 68.48 $mg{\cdot}g^{-1}$ at 318 k, confirming the strong adsorption energy between fluorine and the active bimetallic sites. Thus, the incorporation of metals into MOF structures presents a viable approach to augment the fluoride removal performance.

Aluminum, a chemically active amphoteric metal, has been widely demonstrated as an effective fluoride remover, particularly through its oxide forms (e.g., Al_2O_3) which serve as conventional defluoridation agents [21]. Wang et al. [22] prepared a novel aluminum-containing organometallic framework, Al-MOF-5, by a hydrothermal method, which showed strong fluoride removal performance at different pH and in the presence of different competing ions. Moreover, lanthanide-based materials have been playing an important role in adsorbent materials due to their strong affinity for anions. For example, Yin et al. [23] synthesized five distinct La-MOFs via a hydrothermal method by combining lanthanum nitrate hexahydrate with five organic ligands, evaluating their fluoride ion adsorption capabilities. Notably, La-BDC, incorporating terephthalic acid as the ligand, exhibited the highest adsorption capacity (171.7 mg/g), demonstrating its potential for efficient water defluoridation. Consequently, this complementary behavior of Al-MOFs and La-MOFs motivates the design of Al—La bimetallic MOFs, which could synergistically combine robust chemical activity of aluminum with exceptional fluoride affinity of lanthanum while maintaining cost-effectiveness [19]. Such hybrid materials may overcome the limitations of single-metal MOFs through enhanced binding sites and improved structural stability.

Although Al-La-MOFs have good adsorption potential, the powder form makes them difficult to recover and may further contaminate water bodies, posing an unpredictable threat to aquatic organisms [24]. Sodium alginate (SA), a naturally occurring polysaccharide, possesses an abundance of reactive functional groups [25]. Its surface is rich in -COOH and -OH groups, enabling the adsorption of metal ions through ion exchange, chelation, and coordination [26]. The MOFs material and sodium alginate were mixed to prepare a bead-like material by the embedding method [27], which not only improves the flexibility and plasticity of the material, but also achieves the purpose of reuse. Here, the high fluoride affinity of Al/La combined with the numerous binding sites provided by the alginate make this compound a promising candidate for efficient and sustainable adsorption of fluorine from water.

Herein, novel composite beads (SAMB) for fluoride removal were prepared through hydrothermal synthesis of bimetallic La-Al-MOFs followed by embedding in sodium alginate matrix to form gel spherical structures: i) to investigate the physicochemical properties of the novel absorbents for fluoride removal, ii) to analyze the adsorption performance under different initial concentrations, pH and interfering ions, as well as the adsorption kinetics and adsorption isotherms, iii) to reveal the adsorption mechanism of the new defluorinating agent. This research offers a theoretical foundation for employing MOF-based materials in aqueous fluoride remediation and presents a practical strategy for mitigating fluorine contamination in water treatment applications.

2. Materials and methods

2.1. Preparation of SAMB

The SAMB was prepared according to the following directions. Solution A was prepared by dissolving $Al(NO_3)_3{\cdot}9H_2O$ (33.76 g) and La $(NO_3)_3{\cdot}6H_2O$ (4.33 g) in 24 mL of dimethylformamide (DMF), and solution B was prepared by dissolving 21 g of H_3BTC in 24 mL of ethanol. Under continuous magnetic stirring, Solution A was then infused dropwise with Solution B. After 30 min of stirring, the mixture was transferred to a hydrothermal autoclave and subjected to a 24 h reaction at 150 °C. The resulting product was thoroughly rinsed with DMF and ethanol in a sequential manner for a total of 9 cycles. Following each rinsing step, the solid was separated by centrifugation at 5000 r/min for 5 min. Then, the purified material was dried at 60 °C, yielding the bimetallic MOF material, La-Al-MOFs. Subsequently, 2 g (1 wt%) of the MOF material was combined with 4 g (2 wt%) of sodium alginate, and then to form a homogeneous precursor solution after magnetically stirring for 4 h. The precursor solution was dripped uniformly into 200 mL of a $CaCl_2$ crosslinking solution (5 wt%) and immersed for 12 h to facilitate complete gelation. The resulting beads were then rinsed multiple times to eliminate residual surface $CaCl_2$, followed by drying at 60 °C. The final product obtained was the bimetallic composite bead material, designated as SAMB.

2.2. Batch adsorption experiments

The fluoride removal properties of SAMB were verified through batch experiments. The concentrations of fluoride solution at 10–30 mg/L was selected to simulate the fluoride levels requiring both in contaminated groundwater [28] and advanced treatment in semiconductor wastewater [8]. To investigate the adsorption rate, 0.03 g of SAMB was accurately weighed into a polyethylene tube, followed by the addition of 30 mL of sodium fluoride solution (pH = 7) at initial concentrations of 10 mg/L, 20 mg/L, and 30 mg/L. The polyethylene tubes were incubated at 25 °C in a thermostatic shaker with continuous agitation at 180 rpm. At predetermined time points, samples were sequentially retrieved. The F^- concentration in the supernatant was quantified by ion chromatography (IC).

To investigate the effect of adsorbent dosage on fluoride adsorption, 0.01 g、0.03 g、0.05 g、0.07 g、0.09 g of SAMB were placed in 50 mL polyethylene tubes, and 50 mL of sodium fluoride solution (pH = 7) with an initial F^- of 10 mg/L. The polyethylene tubes were then placed on a constant temperature shaker at 25 °C and shaken at 180 rpm for 24 h to achieve adsorption equilibrium; To ensure robust performance in diverse water chemistries, the adsorbent was tested across a wide pH range (2−12). This range encompasses the acidic conditions of semiconductor or metal plating wastewater, the near-neutral pH of contaminated groundwater, and the alkaline environment of industrial flue gas scrubbing blowdown, thereby confirming its broad applicability

[29]. Specifically, 30 mL of sodium fluoride solution (10 mg/L) was added to a polyethylene tube containing 0.03 g of SAMB with pH ranging from 2 to 12. The tubes were incubated in a thermostatic shaker at 25 °C with agitation at 180 rpm until adsorption equilibrium was attained. Under the same conditions, specific amounts of NaCl, Na_2SO_4, $NaHCO_3$, Na_2CO_3, $NaNO_3$, Na_3PO_4, and $CaCl_2$ were weighed and added to a sodium fluoride solution (pH = 7) with F^- of 10 mg/L.

In order to investigate the adsorption kinetics of the adsorbent, 0.03 g of SAMB was placed in a 50 mL polyethylene tube, and 30 mL of sodium fluoride solution (pH =7) with initial concentrations of 10 mg/L, 20 mg/L, and 30 mg/L was added. At fixed time points (30 min, 1 h, 2 h, 4 h, 6 h, 8 h, 12 h, 16 h, 20 h, 24 h, 30 h, 36 h, 48 h), the water sample was withdrawn to measure the F^- concentration in the supernatant; For the assessment of adsorption isotherm, a portion of 0.03 g of SAMB and 30 mL of sodium fluoride solution (initial F^-: 0 to 150 mg/L) were combined and agitated in a thermostatic shaker. The tubes were incubated in a thermostatic shaker operating at 180 rpm and set to 25 °C, 35 °C, and 45 °C for 24 h. Prior to determining the fluoride concentration, a supernatant sample was membrane-filtered (0.22 μm). All experimental batches, along with the respective blank controls, were performed in parallel and repeated a minimum of three times to confirm the reproducibility and reliability.

2.3. Analysis methods

Thermo dionex aquion ion chromatography analysis system was used to determine F^- concentration with a Dionex IonPac AS11-HC Anion chromatography column (4 × 250 mm) and an elution generator cartridge potassium hydroxide. The pH at the point of zero charge (pH_{zpc}) for the sodium alginate-La-Al-MOFs composite beads was determined using the pH drift method [30]. The surface morphology and elemental composition of SAMB were characterized using scanning electron microscopy (SEM, JSM-7800F) coupled with an energy dispersive spectrometer (EDS). The functional groups of SAMB were examined using a Nicileti S10 Fourier-transform infrared (FTIR) in the range between 4000 cm^{-1} and 400 cm^{-1}. X-ray photoelectron spectroscopy (XPS) analysis was conducted using a Scientific K-Alpha spectrometer (Thermo, USA) to examine the elemental composition. The crystalline properties of SAMB were analyzed using a Quanta 200 X-ray Diffractometer (XRD) under 10–80 degrees. The specific surface area and pore size of SAMB were determined using a Tristar II 3020 Brunauer-Emmett-Teller (BET) surface analyzer under a N_2 atmosphere at a low temperature (77 K) condition. The adsorption material was first subjected to vacuum degassing at 150 °C for 10 h, and then the N_2 adsorption equilibrium values were measured at different pressures. The sample was degassed under IUPAC-recommended conditions [31]. Moreover, the average pore size and the N_2 adsorption-desorption curve of the material were investigated.

2.4. Regeneration of adsorbent

The reusability of SAMB was evaluated by adding 30 mL sodium fluoride solution (10 mg/L) to 0.03 g of the material in a 50 mL polyethylene tube. To ensure full adsorption equilibrium was attained, the samples were continuously shaken for 24 h under controlled conditions (25 °C, 180 rpm) in a thermostatic chamber. Following drying of the solid adsorbent, 30 mL Na_2CO_3 (0.01 mol/L) was introduced, and then desorption process was conducted under identical shaking conditions. Finally, the solid material was rinsed until the effluent reached achieved neutrality. The regeneration of fluoride-laden adsorbents using Na_2CO_3 is a synergistic desorption process. This process is primarily driven by the displacement of F^- with highly concentrated CO_3^{2-} and HCO_3^-, supplemented by the competitive exchange with OH^- under high pH conditions, thereby enabling the cyclic reuse of the adsorbent. The washing cycle was repeated four times, a well-justified number based on previous research [32–34], to assess the adsorption performance by revealing clear trends.

3. Results and discussion

3.1. Characterization of adsorbents

Fig. 1a displays the optical image of the SAMB in wet state, showing a homogeneous smooth spherical morphology with an average diameter of 2.0 ± 0.3 mm. Upon drying (Fig. 1d), the SAMB transforms into rigid spheres with improved mechanical strength and three-dimensional structural support. From Fig. 1b and e, the synthesized bimetallic MOF composite bead (SAMB) clearly displays a rough surface morphology characterized by irregular folded structures and depressions. This structural feature enhances its suitability for adsorbing fluoride ions from aqueous solutions. Furthermore, a noticeable change on the surface after adsorption was observed (Fig. 1c and f), accompanied by the appearance of a flocculent new material, suggesting successful fluoride uptake and the formation of flocculent substances resulting from the interaction of F^- with active sites on the SAMB surface. The EDS pattern demonstrated a uniform distribution of dominant elements La, Al, C, and O on the SAMB surface, a feature that facilitates uptake of fluoride ions (Fig. 1g). Among them, the weight percentages of Al and La elements were found to be 20.96 % and 2.29 % respectively, with a ratio of Al:La = 9.15:1, indicating a composition ratio close to the synthesis method (9:1). The remaining C (30.39 wt%) and O (60.76 wt%) belong to the organic functional groups in the MOF.

Fig. 2 presents the N_2 adsorption-desorption curve and the corresponding BJH pore size distribution profile for the SAMB material. From Fig. 2a, the isotherms correspond to iv-type with H3 hysteresis loops (IUPAC) [35], suggesting the existence of fissure-like pores on the surface of SAMB. The specific surface area and total pore volume were determined to be 3.197 m^2/g and 0.0148 cm^3/g, respectively. The adsorption capacity rose steadily in correlation with rising relative pressure (P/P_o) until it reached saturation, which suggested an extensive pore size distribution [36]. The corresponding pore size distribution profile (Fig. 2b) reveals a broad distribution of mesopores of SAMB, with a peak maximum at 2.78 nm. This pore size is significantly larger than the kinetic diameter of the fluoride ion (0.133 nm), confirming the physical accessibility of the pore network for fluoride adsorption.

Furthermore, the elemental composition, crystalline structure and main functional groups of SAMB before adsorbing were analyzed. The comparison before and after the SAMB adsorbed F^- were described in detail in Section 3.5 (Fig. 7). The XPS scanning spectrum shows that the composite system contains the four fundamental elements C, O, Al, and La. These peaks indicate that La has successfully chemically bonded to Al-MoFs, forming the LA-Al-MoFs structure. The crystalline properties of SAMB were systematically characterized by XRD analysis. The presence of sharp diffraction peaks indicated good crystallization of the adsorbent. The predominant diffraction peaks were observed at 2θ = 9.59°, 36.5°, and 43.6°, representing La-MOFs and Al-MOFs respectively, with the strongest peak at 2θ = 29.9° possibly corresponding to La-Al-MOFs [37]. FTIR analysis characterized the surface functional groups of the adsorbent, with spectra collected over the range of 4000 cm^{-1} to 400 cm^{-1}. SAMB has a rich array of functional groups, such as stretching vibrational peaks of -OH at 3400 cm^{-1}, stretching vibrational peaks of aromatic C═C around 1600 cm^{-1}, and characteristic peaks of La—O, La-OH, Al—O, and Al-OH at 500–1050 cm^{-1} [19].

3.2. Adsorption performance

3.2.1. Effect of adsorbent dosage

Fig. 3a demonstrates how the SAMB dosage affects fluoride removal. It was found that a progressive reduction in the F^- adsorption of SAMB as the adsorbent dosage increases. This trend can be explained by the reduced equilibrium fluoride concentration in solution at higher adsorbent loadings, which diminishes the driving force for adsorption

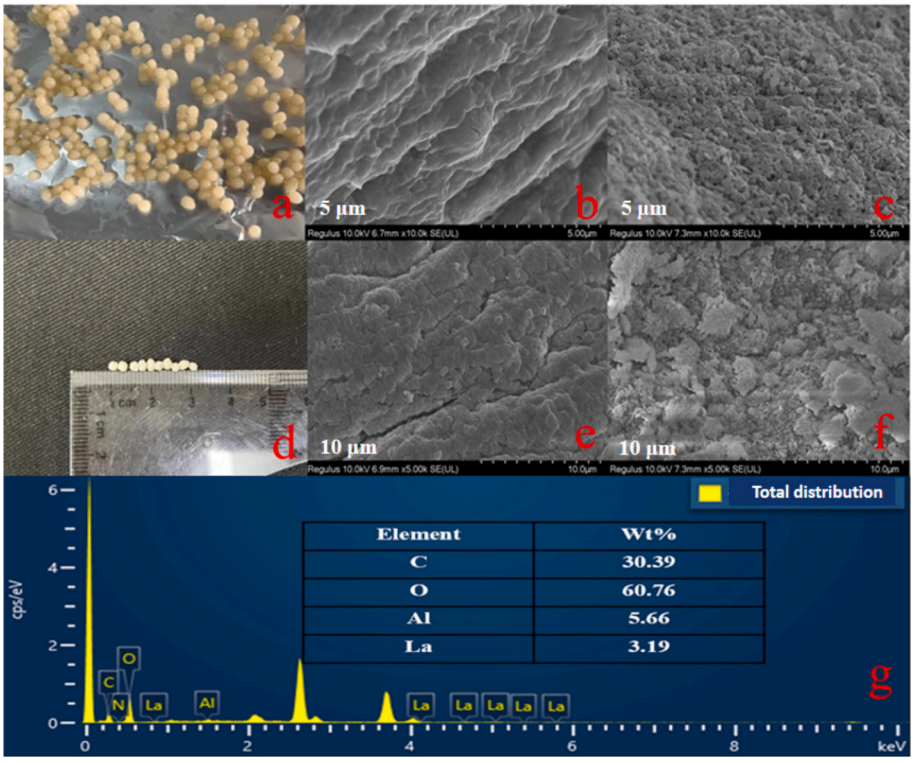

Fig. 1. The wet-state optical image of SAMB (a); the optical image after drying (d); SEM images of SAMB before (b, e) and after adsorption (c, f); EDS analysis of SAMB (g).

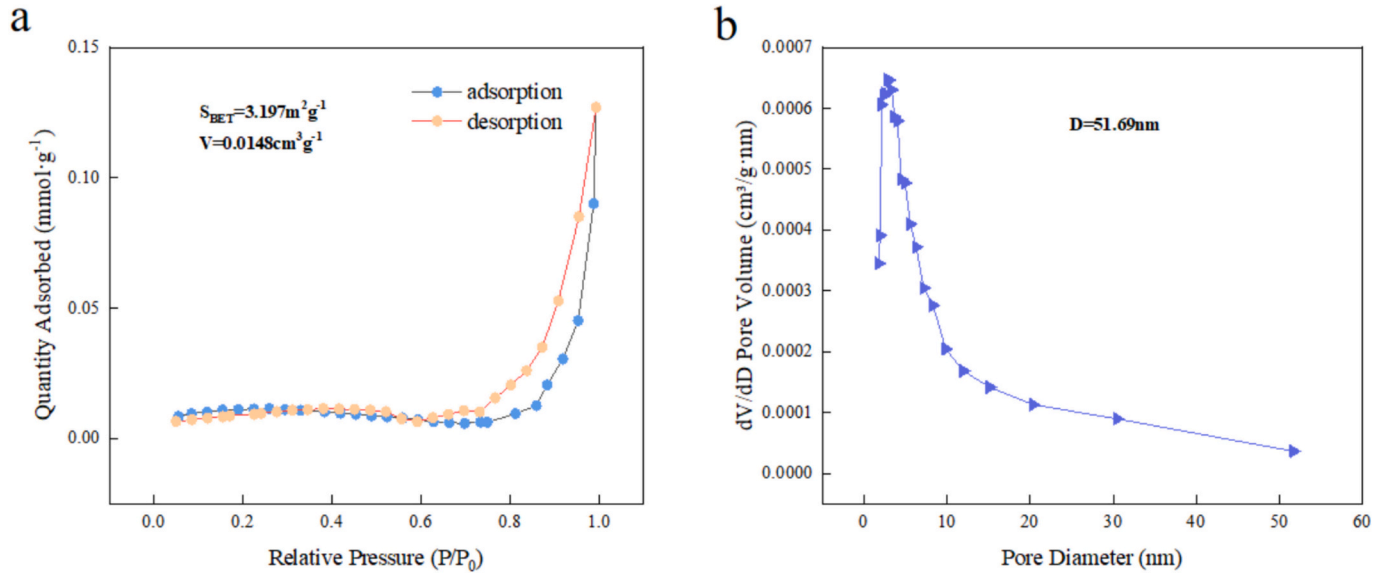

Fig. 2. N_2 adsorption–desorption isotherms (a); corresponding pore size distribution of SAMB (b).

[38]. The fluoride removal efficiency reached 94.6 % under the SAMB dosage of 1 g/L. Near-complete removal (>99 %) was achieved with further increases in dosage, a result ascribed to the higher density of accessible adsorption sites. Therefore, a standard adsorbent concentration of 1 g/L was employed in subsequent experimental works based on optimization of removal efficiency.

3.2.2. *Effect of pH*

Variations in pH significantly influence fluoride ion removal, primarily by modulating the acid-base equilibrium, solubility, and chemical reactivity of coexisting species. Consequently, optimizing the aqueous pH is essential to enhance F^- removal. From the results of Fig. 3b, the optimal fluoride removal efficiency (87.6 %) was achieved under pH of 3. As the pH increased, the F^- removal efficiency gradually decreased and tended to stabilize. When the pH rose to 7, the F^- removal efficiency of SAMB basically stabilized at around 60 %. Furthermore, the removal efficiency exhibited a progressive decline as pH values increased, a trend that aligns with the pH_{pzc} (5.39) of the adsorbent (Fig. 3c). The adsorption of fluoride anions is governed by the interplay between the adsorbent's surface charge and the ionization state of its

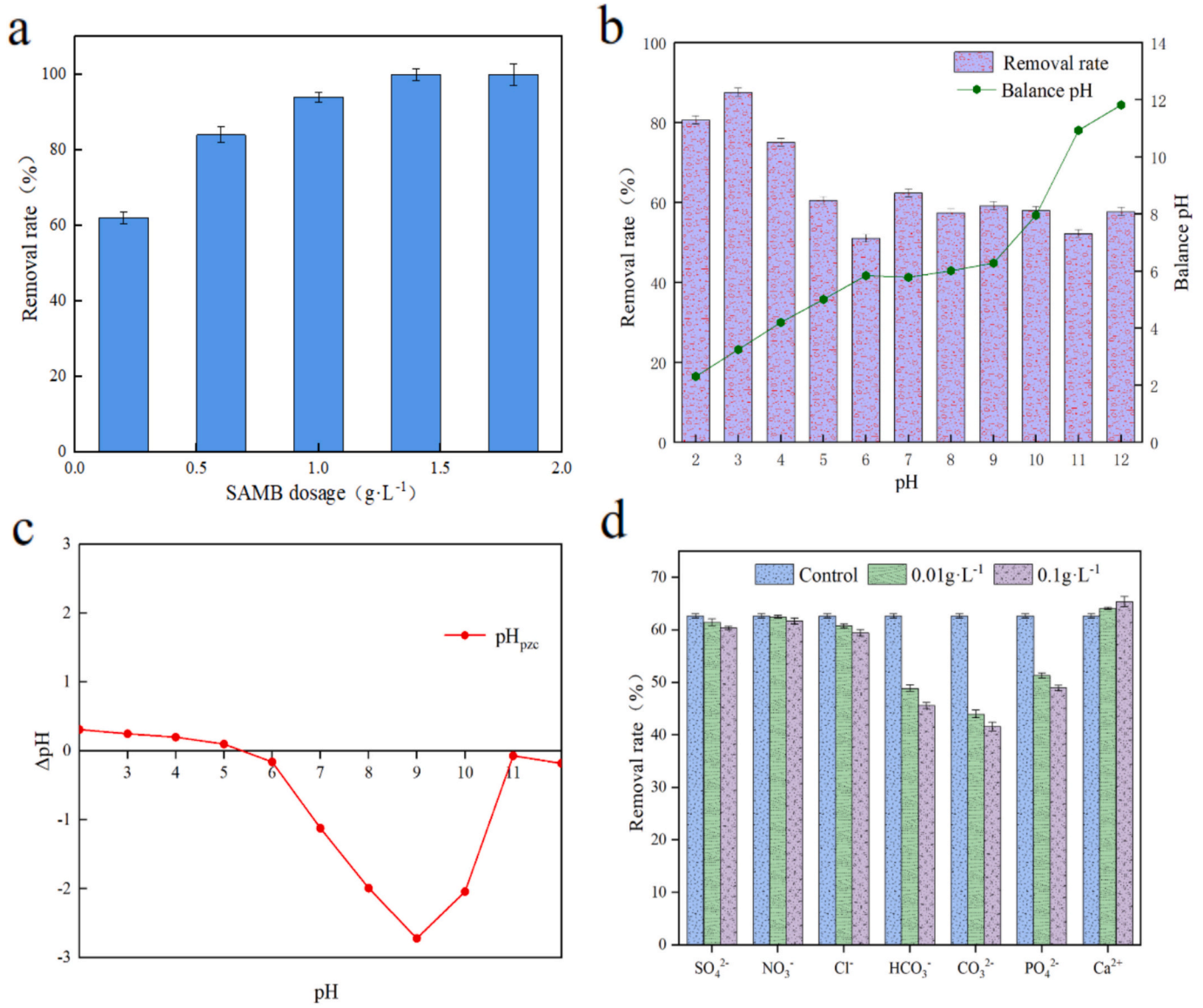

Fig. 3. Effect of adsorbent dosage (a) and solution pH on fluoride removal (b); pH_{pzc} of SAMB material (c); Effect of co-existing ions on fluoride removal (d).

functional groups. Under conditions where the solution pH is below the pH_{pzc}, the adsorbent surface gains a positive charge, thereby promoting the electrostatic attraction and adsorption of fluoride anions. In contrast, under conditions where the pH rises above the pH_{pzc}, the adsorbent surface charge turns negative, leading to electrostatic repulsion against F^- [39]. Furthermore, elevated OH^-concentrations compete with fluoride for the remaining active sites, collectively leading to a significant decrease in removal capacity [40]. Consistent with the observation by Wang et al. (2026), a lower pH enhances fluoride adsorption, owing to promoted electrostatic attraction between the anions and the SAMB surface [28].

3.2.3. *Effect of co-existing ions*

In practical treatment scenarios, where aqueous environments are typically complex, so the competitive effects of common coexisting anions on fluoride removal performance were evaluated. As demonstrated in Fig. 3d, fluoride removal efficiency remained largely unaffected by the presence of these competing anions at concentrations of 0.01 g/L and 0.1 g/L. However, the introduction of HCO_3^-, CO_3^{2-}, and PO_4^{2-} significantly inhibited fluoride adsorption, with the interference effect exhibiting dose-dependent behavior. This competitive adsorption arises through distinct mechanisms: HCO_3^- directly competes with fluoride for surface sites, while the divalent anions (CO_3^{2-} and PO_4^{2-}) form ion pairs with fluoride (CO_3^{2-}-F^- and PO_4^{2-}-F^-) through electrostatic interactions. These complexes reduce the effective concentration of free fluoride ions available for adsorption, thereby decreasing overall removal efficiency [41]. Furthermore, the hydrolysis of these anions generates OH^- in solution, which diminishing the overall removal efficiency vie with F^- for accessible adsorption sites [42]. Additionally, at higher fluoride concentrations, the adsorbent surface imparts a negative charge due to F^- accumulation. Repulsive forces arising from this like-negative charge interaction between the adsorbent surface and F^- further degrade adsorption performance [43].

3.3. *Adsorption model analysis and performance comparisons*

3.3.1. *Adsorption kinetics*

To understand the F^- adsorption behavior of SAMB, kinetic experiments were carried out. F^- could be rapidly adsorbed within 15 min on account of the abundance of active sites on SAMB surface. As the available adsorption sites became increasingly saturated, the rate of adsorption declined and eventually plateaued, reaching equilibrium at

150 min (Fig. 4a). The highest adsorption efficiency of 86 % was observed at the F^- of 10 mg/L. A gradual decrease in adsorption efficiency was observed with increasing initial F^- concentrations, attributable to the limited availability of effective adsorption sites on the adsorbent at higher solute concentrations. SAMB adsorption was fitted by three kinetic models: proposed primary kinetic model, proposed secondary kinetic model and particle diffusion model. The high correlation coefficient ($R^2 > 0.993$) between SAMB's adsorption behavior and the pseudo-second-order model (Fig. 4b and c) is indicative of a adsorption mechanism governed by chemical processes [44]. The adsorption process, according to the intraparticle diffusion model, is characterized by three distinct stages. The initial stage involves rapid surface diffusion, during which a majority of F- are adsorbed onto the adsorbent's exterior (Fig. 4d). The second stage is intrapore adsorption, where most of the adsorption sites have been occupied by fluoride ions, resulting in increased inter-ion competition and a slower adsorption rate. The final stage represents adsorption equilibrium. Collectively, these three stages demonstrate that F- adsorption is a multi-stage process governed primarily by ion diffusion [45].

3.3.2. *Adsorption isotherm and thermodynamic analysis*

The Langmuir and Freundlich isotherm models were applied to model the adsorption behavior of fluoride. Fig. 5a shows that the Langmuir isotherm ($R^2 = 0.98$) exhibited a stronger correlation with the data than the Freundlich isotherm ($R^2 = 0.86$). The fitting results showed a stronger alignment with the Langmuir model, corresponding to homogeneous monolayer adsorption, which was consistent with previous studies [2,46].

According to Fig. 5b, the maximum adsorption value of the SAMB adsorbent at 298.15 K was calculated from Langmuir adsorption isotherm model as $q_{max} = 46.67$ mg/g and a minor enhancement in adsorption capacity was noted as the temperature rose, indicating that elevated temperatures facilitate the reaction kinetics. The corresponding thermodynamic parameters are summarized in Table 1. The negative values of ΔG^0 (−1.65 kJ/mol, −2.05 kJ/mol and − 2.34 kJ/mol) at 298.15 K, 308.15 K, and 318.15 K confirm that the adsorption is spontaneous. The decrease in ΔG^0 with increasing temperature implies that higher temperatures further favor the spontaneity of the adsorption process. The positive value of ΔH^0 (10.28 kJ/mol) indicates an endothermic adsorption reaction, while the positive ΔS^0 (0.04 J/mol/K) suggests an increase in freedom at the solid-liquid interface during fluoride uptake [47].

Moreover, the Langmuir constant K reflects the affinity between the adsorbed substance and the adsorption site. A higher Langmuir constant means that the adsorbed substance is more readily adsorbed onto the material. In conformity with the Langmuir model, the adsorption isotherm can be represented by the subsequent equation:

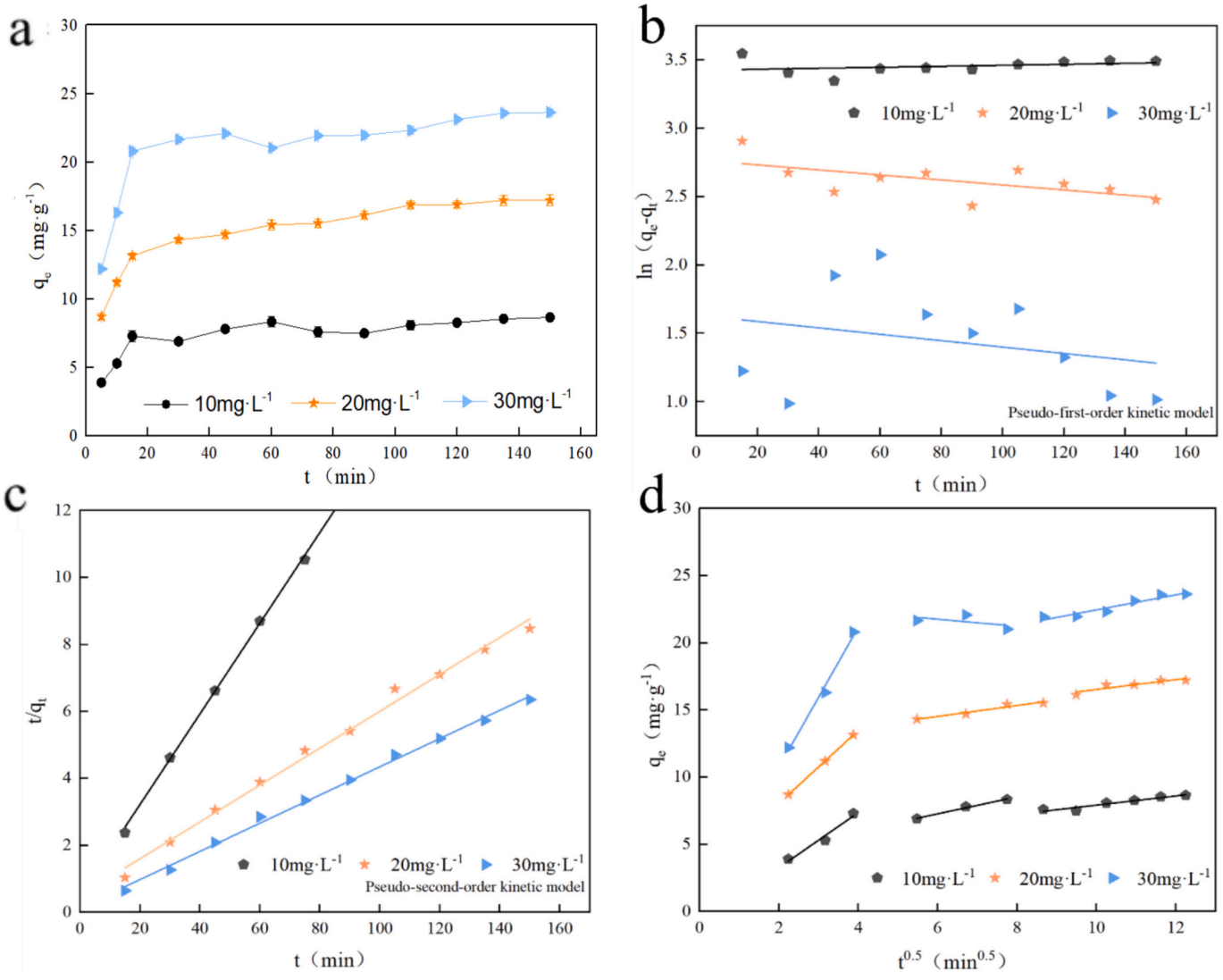

Fig. 4. Adsorption process (a); Pseudo-first-order model (b); Pseudo-second-order model (c); Intra-particle diffusion model for fluoride adsorption on SAMB (d).

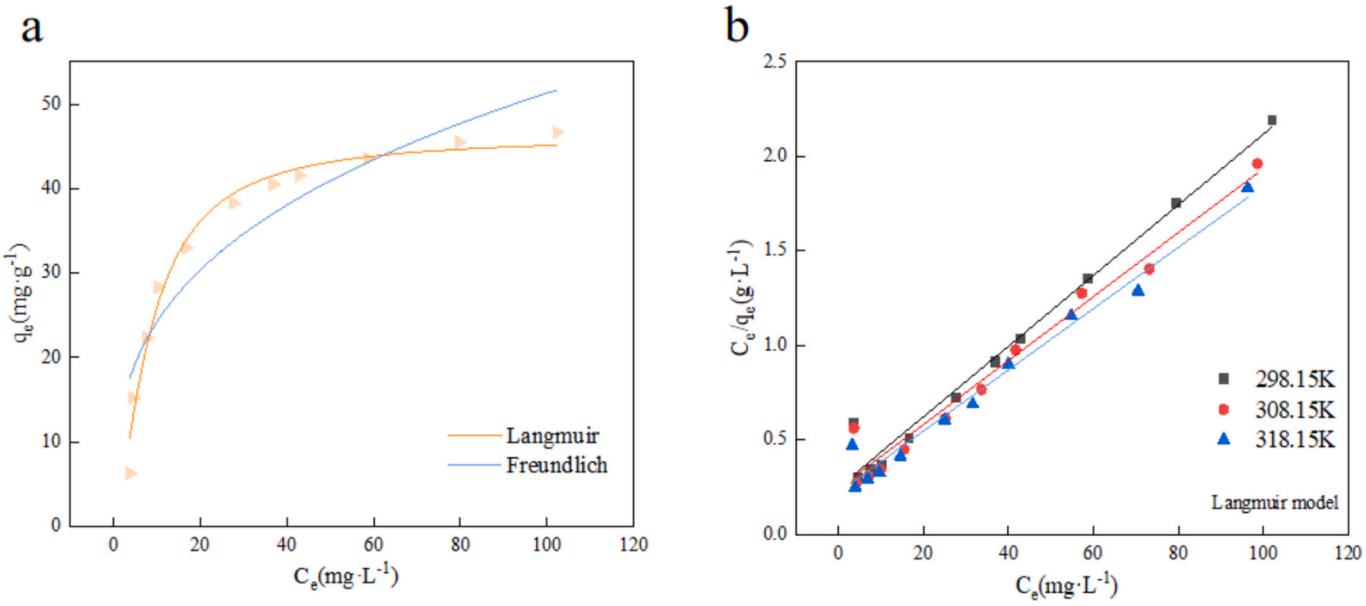

Fig. 5. Adsorption isotherms modeled with the Langmuir and Freundlich models (a); Maximum adsorption capacity of SAMB from Langmuir model (b).

Table 1
Thermodynamic coefficients of F^- adsorption at different temperatures.

T (K)	ΔG° (kJ/mol)	ΔH° (kJ/mol)	ΔS° (J/mol/K)
298.15	−1.65		
308.15	−2.05	10.28	0.04
318.15	−2.34		

$$\theta = (K^* P)/(1 + K^* P)$$

Langmuir constant K value of SAMB was 0.04211 which showed that it adsorbs fluoride ions better.

3.3.3. Comparison with other adsorbents

A systematic comparison with previously reported adsorbents enables a more rigorous assessment of the fluoride removal capability of the SAMB material. As shown in Table 2, the alginate-La-Al-MOFs adsorbent (SAMB) possesses distinct advantages over carbon-based materials, mineral-based substances, and other metal oxides. The q_{max} of SAMB reached 46.67 mg/g, reflecting its high adsorption potential. Furthermore, it maintains effective adsorption across a broad pH range, indicating strong environmental adaptability. In addition, SAMB achieves adsorption equilibrium within only 15 min with adsorption rate among the highest. In summary, SAMB combines high adsorption capacity, wide pH applicability, and rapid adsorption kinetics, rendering it an efficient adsorbent for F^- removal.

Table 2
Comparison of fluoride removal capacity with other adsorbents.

Adsorbent	q_{max} (mg/g)	pH	Time (min)	Ref.
Fe@ABDC MOF	4.92	3–11	30	[48]
Fe_3O_4@CSH-AAO	6.67	2–11	60	[49]
CS/PVA-La-Zr	30.37	3–9	15	[50]
Fe-Al-Mn@CS	40.0	3.5–8.5	45	[51]
ZrS/GPCS-3	44.44	4–10	420	[52]
Al-MOF-PUF@BC	16.52	5.5	/	[21]
ALCS-Fe-Al	30.49	4–9	30	[53]
Mg-Al-Zr triple-metal composite	22.9	3–10	400	[54]
Al-MOFs	39.8	2–12	20	[37]
cerium/iron-based zeolite	45.68	2–12	500	[11]
CS/β-CD aerogel/CSBC/ $MnFe_2O_4$/Al-La MOF	38.59	2–9	50	[55]
Zr-MOF-801	19.42	2–10	30	[13]
Fe_3O_4@MOF-Co@CNF	45.0	2–12	160	[56]
Alginate-La-Al-MOFs	46.67	2–12	15	This study

3.4. Regeneration

Regenerability serves as a critical performance metric for assessing adsorbent applicability. Effective regeneration not only significantly reduces operational costs but also minimizes secondary pollution risks associated with spent adsorbent disposal. The regeneration performance of SAMB was evaluated through multiple adsorption-desorption cycles. It was found from Fig. 6, the material maintained 71 % after three regeneration cycles, indicative of excellent reusability and stable adsorption performance. The desorption ratio of F^- after three cycles was 9.1 %, 20.2 % and 41.0 %, respectively. The corresponding F^- concentrations in the regeneration solution were 2.72 mg/L, 3.62 mg/L, and 5.28 mg/L. The gradual decline in adsorption capacity across cycles

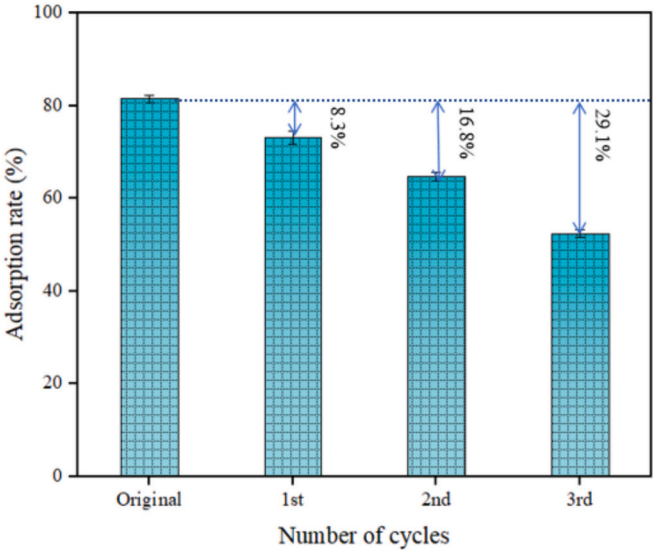

Fig. 6. Recyclability of SAMB on fluoride adsorption.

is likely attributable to several interrelated factors. First, incomplete desorption of fluoride ions may lead to partial occupation of active sites, thereby limiting their availability in subsequent cycles. Furthermore, repeated chemical and thermal stresses during regeneration may cause structural degradation, such as partial pore collapse or damage to key functional groups, which would diminish the intrinsic adsorption capacity of the material [56]. On the whole, the adsorbent demonstrated consistent fluoride ion adsorption efficiency across multiple cycles, coupled with effective fluoride release during desorption, thereby maintaining its high adsorption capacity and performance. This cyclic stability suggests the material possesses optimal surface characteristics, including abundant active sites, favorable pore architecture, and strong ion-exchange capability, all of which contribute to enhanced fluoride removal efficiency.

3.5. Removal mechanisms of fluoride

The results of SEM imaging (Fig. 1) and BET analysis (Fig. 2) revealed a hierarchical porous architecture featuring interconnected macropores and mesopores, which provide substantial surface area and pore volume for effective fluoride ion adsorption [57]. F^- are adsorbed into the pores through a combination of physical interactions and chemical binding, leading to their immobilization within the framework [58]. Moreover, the oxygen and nitrogen atoms present in the organic ligands of La-Al-MOFs facilitate fluoride retention by engaging hydrogen bonds with the target ions [59]. This not only increases fluoride adsorption capacity but also ensures more stable immobilization of the ions on the material's surface. Additionally, it was found that the SAMB adsorption process correlated most strongly with the pseudo-second-order kinetic (Fig. 4) and Langmuir isotherm models (Fig. 5), confirming monolayer chemisorption as the dominant mechanism [50].

The XPS results of SAMB as shown in Fig. 7a, revealing that the basic surface elements remain the same, while the emergence of a new F 1 s at 685.2 eV post-adsorption validates the successful binding of F^- to the material. Fig. 7b shows a detailed map of C 1 s, where characteristic peaks observed at 284.6 eV (C—C) and 288.0 eV (C=O). Following adsorption, a noticeable transformation from C—C to C=O bonds was detected, pointing to a notable interaction between the adsorbent and F^-, potentially involving electron transfer. A shift to higher binding energies was observed in the La 3d peaks after adsorption, with the La $3d_{3/2}$ and La $3d_{5/2}$ peaks moving to 835.3 eV and 838.2 eV from their original positions at 831.5 eV and 836.3 eV, respectively (Fig. 7c). This

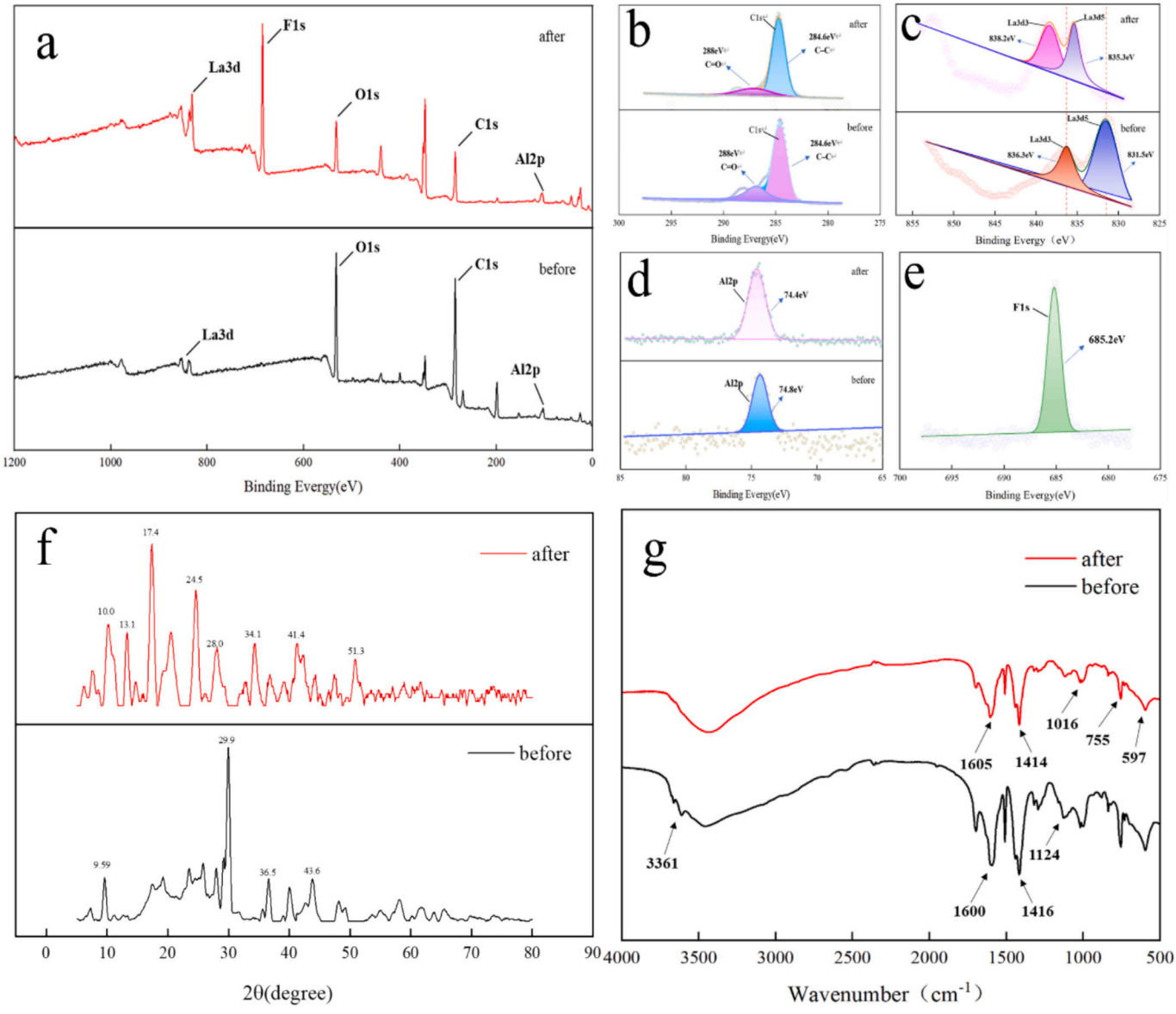

Fig. 7. XPS spectra: survey spectra (a), C 1 s(b), La 3d(c), Al 2p(d), F 1 s of SAMB (e); XRD pattern(f), FTIR spectra of SAMB(g).

result confirmed the participation of La in fluoride adsorption, primarily via a ligand exchange process that facilitates La—F bonding. The peaks of Al 2p in Fig. 7d, appearing at 74.4 eV to 74.8 eV, indicated the presence of trivalent aluminum oxide. A decrease in the Al binding energy from 74.8 eV to 74.4 eV was observed post-adsorption, corresponding to a notable interaction with F^-. The adsorption process of the adsorbent was further examined using XRD. Fig. 7f displays the XRD patterns of the SAMB, and the appearance of new peaks post-adsorption, such as 51.3° for $La(COOH)_3$, was related to the specific metal-fluoride interactions [60]. The presence of additional diffraction peaks demonstrated interactions between metal moieties and fluoride, along with successful incorporation of fluoride into the lattice [61].

As presented in Fig. 7g of FTIR, the stretching and bending vibrations observed at 3361 cm^{-1} and 1124 cm^{-1} in the SAMB spectrum are associated with surface water and hydroxyl groups, respectively, indicating the ionic exchange between F^- and OH^- on SAMB [62]. A noticeable weakening and shift of the peaks from 1697 cm^{-1} to 1605 cm^{-1} and from 1416 cm^{-1} to 1414 cm^{-1} is observed, suggesting a modification in the C═C and COOH stretching vibrations, potentially due to substitution effects [36]. Additionally, the substitution of hydrogen atoms on the benzene ring, caused by the strong electronegativity of F^-, breaks the central symmetry of the benzene ring molecule, leading to unequal electron densities among the six carbon atoms on the benzene ring and leading to a displacement of the peak positions [63]. The absorption bands in the 500–1050 cm^{-1} range are characterized by La—O, La-OH, Al—O, and Al-OH vibrational modes, respectively. These peaks was notably reduced following the adsorption process, indicating successful adsorption of F^-. The decay or disappearance of the post-adsorption metal-dependent characteristic peak has been attributed to electrostatic interactions between F^- and M-OH^{2+}. Thereby, it can be inferred from this that the adsorption of F^- is primarily achieved through electrostatic adsorption and ion exchange [46].

Overall, the adsorption mechanism involves multiple processes. First, both La and Al in the adsorbent exhibit strong affinity for fluoride ions (F^-) [64]. Given that F^- and OH^- share similar ionic radii and electronegativity values, efficient ion exchange occurs between surface hydroxyl groups (-OH) and aqueous F^- when they come into contact. This exchange mechanism was confirmed by FTIR and XRD analyses, which showed clear evidence of -OH/F^- substitution. Additionally, SAMB demonstrates notable reactive adsorption capacity, further contributing to fluoride removal through chemical interactions [65].

The fluoride adsorption mechanism involves both chemical and electrostatic interactions. A portion of fluoride ions undergo chemisorption at active sites, forming stable metal-fluoride or organo-fluoride compounds, thereby enhancing both adsorption capacity and ion selectivity [66]. Surface charge analysis revealed a pHpzc of 5.39 for SAMB, indicating critical pH-dependent behavior: (i) At pH < 5.39, protonation generates a positively charged surface that electrostatically attracts F^- anions, promoting adsorption; (ii) At pH > 5.39, surface deprotonation creates negative charges that repel F^-, reducing adsorption efficiency due to diminished electrostatic attraction [67]. Collectively, these results demonstrate that SAMB's fluoride removal mechanism operates primarily through synergistic electrostatic attraction and ion exchange (Fig. 8). The multi-mechanistic adsorption process entails the following steps:

$$La/Al - OH_2^+(s) \rightarrow La/Al - F^-(s) + H_2O$$

$$La/Al - OH^+(s) \rightarrow La/Al - F^-(s) + OH^-$$

4. Conclusions

Herein, a bead-like adsorbent, SAMB, was manufactured via the entrapment of a bimetallic MOF in a sodium alginate hydrogel for enhanced fluoride remediation. The SAMB material exhibited broad pH adaptability for fluoride adsorption, with optimal removal efficiency achieved at pH 3. Thermodynamic and kinetic analyses indicated a monolayer adsorption mechanism dominated by chemisorption, as evidenced by the optimal fit to the pseudo-second-order kinetic and Langmuir isotherm models. Comprehensive characterization through SEM, FTIR, BET, XRD, and XPS analyses elucidated an adsorption mechanisms governed principally by ion exchange and electrostatic interactions. Furthermore, regeneration experiments confirmed the material's excellent reusability. The synthesized SAMB material demonstrates significant potential as an eco-friendly adsorbent, providing an effective and sustainable approach for mitigating fluoride contamination in aqueous environments. Future studies will focus on validating the performance in real semiconductor wastewater, evaluating the long-term stability and reusability of SAMB materials, and determining selectivity in complex matrices.

CRediT authorship contribution statement

Zi Song: Writing – original draft, Methodology, Investigation, Formal analysis, Data curation. **Ze Wang:** Validation, Investigation, Formal analysis, Data curation. **Fei Yang:** Writing – review & editing, Resources, Project administration, Funding acquisition. **Huu Hao Ngo:** Writing – review & editing, Validation, Supervision, Conceptualization. **Wenshan Guo:** Writing – review & editing, Visualization, Validation, Data curation. **Xinbo Zhang:** Writing – review & editing, Supervision,

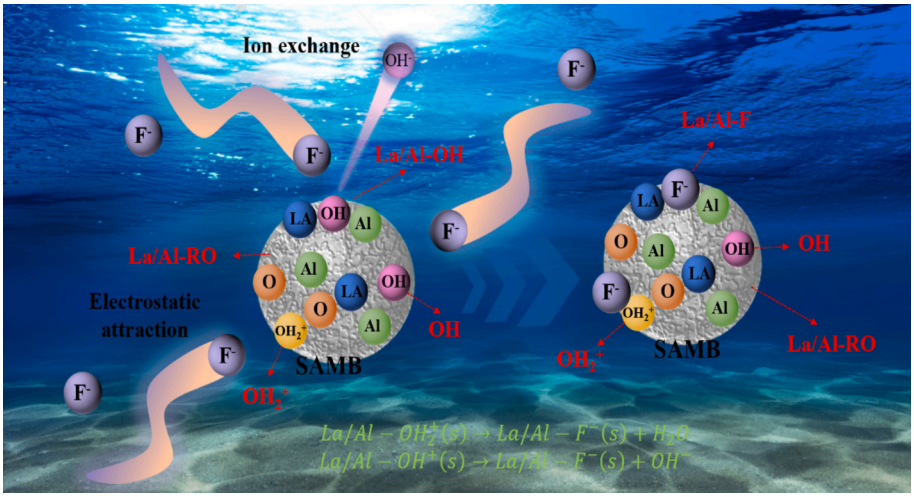

Fig. 8. Schematic of adsorption mechanism for defluoridation.

Resources, Project administration, Methodology, Conceptualization.

Declaration of competing interest

The authors declare that they have no known competing financial interests or personal relationships that could have appeared to influence the work reported in this paper.

One of the co-authors of this article, Prof. Wenshan Guo, is currently an Editor of JWPE.

Acknowledgements

This research was supported by Tianjin Municipal Science and Technology Bureau (No.25JCZDJC00240), and the National Natural Science Foundation of China (No.52500090 and No.52400054).

Data availability

No data was used for the research described in the article.

References

[1] J. He, Y. Yang, Z. Wu, C. Xie, K. Zhang, L. Kong, J. Liu, Review of fluoride removal from water environment by adsorption, J. Environ. Chem. Eng. 8 (6) (2020) 104516.
[2] P.N. Thakre, S. Mukherjee, S. Samanta, S. Barman, G. Halder, A mechanistic insight into defluoridation of simulated wastewater applying bio-inspired sodium alginate bead, Appl Water Sci 10 (2) (2020) 65.
[3] J. Chen, R. Yang, Z. Zhang, D. Wu, Removal of fluoride from water using aluminum hydroxide-loaded zeolite synthesized from coal fly ash, J. Hazard. Mater. 421 (2022) 126817.
[4] X. Wang, H. Pfeiffer, J. Wei, J. Dan, J. Wang, J. Zhang, 3D porous ca-modified Mg-Zr mixed metal oxide for fluoride adsorption, Chem. Eng. J. 428 (2022) 220–231.
[5] X. Dai, T. Qi, X. Li, Z. Peng, G. Liu, Q. Zhou, Y. Wang, L. Shen, Efficient removal of fluorine in sodium aluminate solution via double salt crystallization process, J. Environ. Chem. Eng. 13 (2025) 115269.
[6] Y. Yang, Z. Yang, X. Liu, L. Qi, Y. Zhou, Z. Zhu, J. Qi, J. Li, Emerging contaminants removal through fluorine-doped carbon hollow fiber microfiltration membrane based on metal-free electro-Fenton, J. Membr. Sci. 715 (2025) 123477.
[7] S.K. Sahoo, G. Hota, Surface functionalization of GO with $MgO/MgFe_2O_4$ binary oxides: a novel magnetic nanoadsorbent for removal of fluoride ions, J. Environ. Chem. Eng. 6 (2) (2018) 2918–2931.
[8] B. Luo, Y. Liu, Y. Yan, H. He, J. Yu, Q. Chen, Research on the removal of fluoride from low-concentration fluorine-containing industrial wastewater using adsorption methods, Biochem. Eng. J. 216 (2025) 109668.
[9] N. Singh, A. Dhillon, D. Kumar, Metal-organic frameworks for adsorption of fluoride for groundwater treatment, Groundw. Sustain. Dev. 23 (2023) 100967.
[10] E. Jeong, S. Jung, H. Shin, Fluorine-functionalized reduced graphene oxide-TiO_2 nanocomposites: a new application approach for efficient photocatalytic disinfection and algicidal effect, Environ. Pollut. 319 (2023) 120974.
[11] F. Li, X. Li, J. Yu, S. Li, L. Guo, C. Xiao, J. Li, Y. Zhang, R. Chi, Enhanced removal of phosphate and fluoride from phosphogypsum leachate by cerium/iron-based zeolite: adsorption behaviors and competition mechanisms, Sep. Purif. Technol. 376 (3) (2025) 134185.
[12] B. Wang, Y. Yin, H. Deng, H. Zhu, G. Li, W. He, Migration, transformation, and management of fluorine-containing substances in lithium-ion batteries during recycling-a review, Sep. Purif. Technol. 358 (A) (2025) 130283.
[13] T.L. Tan, P.A/.P. Krusnamurthy, H. Nakajima, S.A. Rashid, Adsorptive, kinetics and regeneration studies of fluoride removal from water using zirconium-based metal organic frameworks, RSC Adv. 10 (2020) 18740–18752.
[14] J. Wang, Y. Sun, X. Zhao, L. Chen, S. Peng, C. Ma, G. Duan, Z. Liu, H. Wang, Y. Yuan, N. Wang, A poly(amidoxime)-modified MOF macroporous membrane for high-efficient uranium extraction from seawater, e-Polymers 22 (1) (2022) 399–410.
[15] G. Cai, P. Yan, L. Zhang, H.C. Zhou, H.L. Jiang, Metal-organic framework-based hierarchically porous materials: synthesis and applications, Chem. Rev. 121 (20) (2021) 12278–12326.
[16] M. Rostami, A. Badiei, M. Alijani, A. Das, G.M. Ziarani, Nanoarchitectonic MOF-derived materials for enhanced photocatalytic activity in organic contaminant removal: a review, Alex. Eng. J. 126 (2025) 448–479.
[17] S. Zhou, X. Chen, Q. Li, L. Huang, X. Qiu, J. Yan, H. Zhang, Q. Zheng, Q. Liu, A comprehensive review of fluoride removal using low-cost adsorbents for environmental and industrial applications, Environ. Surf. Interfaces 3 (2025) 146–162.
[18] H. Ma, Y. Huang, J. Tang, W. Wang, B. Liu, H. Sun, S. Yang, G. Han, Enhanced fluoride removal via adsorption flotation based on La-MOF carrier morphology modulation strategy, Sep. Purif. Technol. 365 (2025) 132652.
[19] S.I. Alhassan, H. Wang, Y. He, L. Yan, Y. Jiang, B. Wu, T. Wang, H. Gang, L. Huang, L. Jin, Y. Chen, Fluoride remediation from on-site wastewater using optimized bauxite nanocomposite (Bx-Ce-La@500): synthesis maximization, and mechanism of F(horizontal line) removal, J. Hazard. Mater. 430 (2022) 128401.
[20] F. Ke, A. Pan, J. Liu, X. Liu, T. Yuan, C. Zhang, G. Fu, C. Peng, J. Zhu, X. Wan, Hierarchical camellia-like metal-organic frameworks via a bimetal competitive coordination combined with alkaline-assisted strategy for boosting selective fluoride removal from brick tea, J. Colloid Interface Sci. 642 (2023) 61–68.
[21] Z. Wang, X. Gu, X. Zhang, X. Wang, J. Zhang, Y. Liu, X. Tan, Y. Zhao, D. Kang, W. Guo, H.H. Ngo, New easily recycled carrier based polyurethane foam by loading Al-MOF and biochar for selective removal of fluoride ion from aqueous solutions, Sci. Total Environ. 901 (2023) 166312.
[22] X. Wang, K. Liu, H. Zhu, T. Sun, T. Han, J. Li, H. Dai, An effective and selective stable metal-organic framework adsorbent (Al-MOF-5) for the removal of fluoride from water, Desalin. Water Treat. 216 (2021) 220–231.
[23] C. Yin, Q. Huang, G. Zhu, L. Liu, S. Li, X. Yang, S. Wang, High-performance lanthanum-based metal-organic framework with ligand tuning of the microstructures for removal of fluoride from water, J. Colloid Interface Sci. 607 (Pt 2) (2022) 1762–1775.
[24] S. Liu, F. Fan, Z. Ni, J. Liu, S. Wang, Sustainable lanthanum-attapulgite/alginate hydrogels with enhanced mechanical strength for selective phosphate scavenging, J. Clean. Prod. 385 (2023) 165351.
[25] S. Shan, H. Tang, Y. Zhao, W. Wang, F. Cui, Highly porous zirconium-crosslinked graphene oxide/alginate aerogel beads for enhanced phosphate removal, Chem. Eng. J. 359 (2019) 779–789.
[26] M. Zeng, W. Wu, J. Fang, Z. Zhou, Y. Lan, B. Lin, Q. Ye, Fabrication of sodium alginate porous scaffolds for heavy metal ion removal from aqueous solution, J. Macromol. Sci. Part B 61 (10−11) (2023) 1350–1365.
[27] A. Wang, K. Zhou, X. Liu, F. Liu, C. Zhang, Q. Chen, Granular tri-metal oxide adsorbent for fluoride uptake: adsorption kinetic and equilibrium studies, J. Colloid Interface Sci. 505 (2017) 947–955.
[28] M. Wang, Y. Luo, T. Tuerhong, Y. Wang, Adsorption of arsenic–fluorine in groundwater by Fe/La-modified wheat straw–derived biochar, Mater. Chem. Phys. 348 (1) (2026) 131606.
[29] R. Wang, C. Zhang, H. Yu, W. Sun, Research progress on hazardous fluorine-containing wastewater treatment in the integrated circuit industry: a resource recovery perspective, Sep. Purif. Technol. 365 (2025) 132626.
[30] V. Aghazadeh, S. Barakan, E. Bidari, Determination of surface protonation-deprotonation behavior, surface charge, and total surface site concentration for natural, pillared and porous nano bentonite heterostructure, J. Mol. Struct. 1204 (2020) 127570.
[31] M. Thommes, K. Kaneko, A.V. Neimark, J.P. Olivier, F. Rodriguez-Reinoso, J. Rouquerol, K.S.W. Sing, Physisorption of gases, with special reference to the evaluation of surface area and pore size distribution (IUPAC technical report), Pure Appl. Chem. 87 (9–10) (2015) 1051–1069.
[32] J. Xu, Y. Peng, M. Chen, G. Wang, Z. Han, X. Chen, Adsorption behavior and mechanisms of nitrogen-doped porous biochar for toluene: a perspective on pore structure and thermal aging resistance, J. Environ. Chem. Eng. 13 (2025) 119739.
[33] C. Zheng, W. Zhang, Z. Zuo, Y. Jin, J. Li, S. Luo, J. Li, Unveiling synergistic effect of potassium permanganate and potassium ferrate to manufacture magnetic biochar by low-temperature pyrolysis for efficient adsorption of tetracycline and copper, Chem. Eng. Sci. 321 (A) (2026) 122745.
[34] K. He, A. Sun, Z. Guo, C. Zheng, Y. Jin, H. Jiang, Y. Xiao, J. Li, Preparation of nano zero-valent iron-doped magnetic biochar from different types of iron salts: comparing their adsorption capability for sulfamethoxazole, J. Environ. Chem. Eng. 13 (2025) 119127.
[35] L. Kong, Y. Tian, N. Li, Y. Liu, J. Zhang, J. Zhang, W. Zuo, Highly-effective phosphate removal from aqueous solutions by calcined nano-porous palygorskite matrix with embedded lanthanum hydroxide, Appl. Clay Sci. 162 (2018) 507–517.
[36] Q. Huang, L. Zhao, G. Zhu, Outstanding performance of thiophene-based metal-organic frameworks for fluoride capture from wastewater, Sep. Purif. Technol. 298 (2022) 121567.
[37] S.A. Ratthika, K. Ramkumar, S.S.D. Elanchezhiyan, R. Kumar, S. Meenakshi, Synthesis and characterization of lanthanum-assisted aluminium metal-organic frameworks for the removal of fluoride ions from an aqueous environment, J. Environ. Chem. Eng. 13 (2025) 118181.
[38] M. Zhao, X. Zhou, J. Li, F. Li, X. Li, J. Yu, L. Guo, G. Song, C. Xiao, F. Zhou, R. Chi, G. Feng, Efficient removal of phosphate and fluoride from phosphogypsum leachate by lanthanum-modified zeolite: synchronous adsorption behavior and mechanism, J. Environ. Chem. Eng. 12 (2024) 113294.
[39] H.N. Tran, S. You, A. Hosseini-Bandegharaei, H.P. Chao, Mistakes and inconsistencies regarding adsorption of contaminants from aqueous solutions: a critical review, Water Res. 120 (2017) 88–116.
[40] H.A.L. de Oliveira, A.F.C. Campos, G. Gomide, Y. Zhang, S. Ghoshal, Elaboration of a core@shell bimagnetic nanoadsorbent (CoFe2O4@γ-Fe2O3) for the removal of as (V) from water, Colloids Surf. A Physicochem. Eng. Asp. 600 (2020) 142113.
[41] Z. Mahdavi, S.J. Peighambardoust, M. Foroughi, R. Foroutan, M. Ahmadi, B. Ramavandi, Enhancing fluoride ion removal from aqueous solutions and glass manufacturing wastewater using modified orange peel biochar magnetic composite with MIL-53, Environ. Res. 262 (2024) 119825.
[42] Z. Wang, J. Su, T. Zhao, J. Li, L. Zhang, Enhanced removal of fluoride from groundwater using biosynthetic hydroxyapatite modified by bimetallic (La–Fe or La–Al) hydroxides, J. Clean. Prod. 436 (2024) 140649.
[43] A. Iizuka, H.J. Ho, A. Yamasaki, Removal of fluoride ions from aqueous solution by metaettringite, PLoS One 17 (3) (2022) e0265451.
[44] J. Zhao, C. Wang, S. Wang, Y. Zhou, Experimental and DFT study of selective adsorption mechanisms of Pb(II) by UiO-66-NH2 modified with 1,8-dihydroxyanthraquinone, J. Ind. Eng. Chem. 83 (2020) 111–122.

[45] J. Hu, J. Song, X. Han, Q. Wen, W. Yang, W. Pan, S. Jian, S. Jiang, Fabrication of Ce-La-MOFs for defluoridation in aquatic systems: a kinetics, thermodynamics and mechanisms study, Sep. Purif. Technol. 314 (2023) 123562.
[46] W. Li, Z. Wang, X. Zhang, Y. Zhang, T. Long, X. Wang, J. Zhang, J. Liu, Tailored design of a novel composite foam of sodium alginate used for fluoride ion removal, Water Sci. Technol. 86 (4) (2022) 643–655.
[47] H.N. Tran, E.C. Lima, R. Juang, J. Bollinger, H. Chao, Thermodynamic parameters of liquid–phase adsorption process calculated from different equilibrium constants related to adsorption isotherms: a comparison study, J. Environ. Chem. Eng. 9 (2021) 106674.
[48] A. Jeyaseelan, M. Naushad, T. Ahamad, N. Viswanathan, Design and development of amine functionalized iron based metal organic frameworks for selective fluoride removal from water environment, J. Environ. Chem. Eng. 9 (2021) 104563.
[49] H. Yang, H. Zhang, J. Lu, Y. Cui, Y. Wang, X. Wang, J. Xue, H. Cao, Advanced magnetic adsorbents for enhanced phosphorus and fluoride removal from wastewater: mechanistic insights and applications, Sep. Purif. Technol. 353 (A) (2025) 128195.
[50] L. Mei, J. Wei, R. Yang, F. Ke, C. Peng, R. Hou, J. Liu, X. Wan, H. Cai, Zirconium/lanthanum-modified chitosan/polyvinyl alcohol composite adsorbent for rapid removal of fluoride, Int. J. Biol. Macromol. 243 (2023) 125155.
[51] M. Chaudhary, S. Rawat, N. Jain, A. Bhatnagar, A. Maiti, Chitosan-Fe-Al-Mn metal oxyhydroxides composite as highly efficient fluoride scavenger for aqueous medium, Carbohydr. Polym. 216 (2019) 140–148.
[52] W. Lu, C. Zhang, Y. Li, Z. Qin, X. Li, Y. Li, K. Zhang, Double cross-linked chitosan sponge encapsulated with ZrO_2/soy protein isolate amyloid fibrils nanoparticles for the fluoride ion removal from water, Int. J. Biol. Macromol. 279 (4) (2024) 135520.
[53] J. Feng, H. Bai, Y. Xue, R. Zhang, P. Zhu, D. Bu, Z. Dan, W. Li, X. Lu, Recycling of iron and aluminum from drinking water treatment sludge for synthesis of a magnetic composite material (ALCS-Fe-Al) to remove fluoride from drinking water, Groundw. Sustain. Dev. 11 (2020) 100456.
[54] M. Wang, X. Yu, C. Yang, X. Yang, M. Lin, L. Guan, M. Ge, Removal of fluoride from aqueous solution by Mg-Al-Zr triple-metal composite, Chem. Eng. J. 322 (2017) 246–253.
[55] R. Foroutan, A. Tutunchi, M. Foroughi, B. Ramavandi, Efficient fluoride removal from water and industrial wastewater using magnetic chitosan/β-cyclodextrin aerogel enhanced with biochar and MOF composites, Sep. Purif. Technol. 363 (2) (2025) 132128.
[56] G. Zhou, Q. Meng, S. Li, R. Song, Q. Wang, Z. Xu, Z. Xing, Novel magnetic metal-organic framework derivative: an adsorbent for efficient removal of fluorine-containing wastewater in mines, J. Environ. Chem. Eng. 10 (2022) 108421.
[57] X. Sun, C. Ke, Q. Lu, L. Liang, G. Xie, Adsorption of fluoride ion on Al/La modified acidified attapulgite composite materials, Sep. Purif. Technol. 354 (2025) 128791.
[58] Y. Zou, D. Diao, H. Zhang, Z. Qiu, Y. Wang, Y. Wang, H. Ding, J. Yang, X. Xiao, Evaluation of the efficient fluoride removal of porous CeO2/HAP: performance and mechanism study, Sep. Purif. Technol. 364 (2025) 132527.
[59] S. Liu, J. Wang, J. Ren, M. Zhang, H. Mao, Environmentally benign tannin-modified chitosan aerogel decorated with Zr(IV) enabled high-performance adsorption of fluoride, Chem. Eng. J. 519 (2025) 165351.
[60] M. Wang, H. Ye, X. Zheng, S. Chen, H. Xing, X. Tao, Z. Dang, G. Lu, Adsorption behaviors and mechanisms of simultaneous cadmium and fluoride removal on waste bovine bone from aqueous solution, J. Environ. Chem. Eng. 11 (2023) 109035.
[61] J. Song, Y. Yu, X. Han, W. Yang, W. Pan, S. Jian, G. Duan, S. Jiang, J. Hu, Novel MOF(Zr)-on-MOF(Ce) adsorbent for elimination of excess fluoride from aqueous solution, J. Hazard. Mater. 463 (2024) 132843.
[62] R. Liu, J. Song, J. Zhao, Z. Wang, J. Xu, W. Yang, J. Hu, Novel MOF(Zr)–on-MOF (Ce/La) adsorbent for efficient fluoride and phosphate removal, Chem. Eng. J. 497 (2024) 154780.
[63] D. Marghade, S. Shelare, C. Prakash, M.E.M. Soudagar, T.M.Y. Khan, M.A. Kalam, Innovations in metal-organic frameworks (MOFs): pioneering adsorption approaches for persistent organic pollutant (POP) removal, Environ. Res. 258 (2024) 119404.
[64] Y. Liu, D. Zhong, Y. Xu, H. Chang, L. Dong, Z. Han, J. Li, N. Zhong, Adsorption of phosphate in water by La/Al bimetallic-organic frameworks-chitosan composite with wide adaptable pH range, J. Environ. Chem. Eng. 11 (2023) 110309.
[65] Y. Chen, B. Zhou, H. Liu, R. Yuan, X. Wang, Z. Feng, Z. Chen, H. Chen, Strategies to improve adsorption and photocatalytic performance of metal-organic frameworks (MOFs) for perfluoroalkyl and polyfluoroalkyl substances (PFASs) removal from water: a review, Environ. Res. 240 (2024) 117483.
[66] F.G. Quintero-Álvarez, D.I. Mendoza-Castillo, M. Almáši, E. García-Hernández, L. Palomino-Asencio, C. Cuautli, C.J. Duran-Valle, M. Adame-Pereira, A. Bonilla-Petriciolet, Lanthanide-based metal-organic frameworks MOF-76 for the depollution of xenobiotics from water: arsenic and fluoride adsorption properties and multi-anionic mechanism analysis, J. Mol. Struct. 1338 (2025) 142113.
[67] F.A. Dar, S. Kurella, Removal of fluoride from wastewater with the Mg/Al impregnated adsorbent prepared from chinar leaves: adsorption isotherm, kinetic and thermodynamic studies, Environ. Res. 271 (2025) 121004.